

Nonequilibrium superconducting thin films with sub-gap and pair-breaking photon illumination

T Guruswamy,* D J Goldie, and S Withington
Quantum Sensors Group, Cavendish Laboratory, University of Cambridge,
J J Thomson Avenue, Cambridge, CB3 0HE, UK

(Dated: November 9, 2021)

We calculate nonequilibrium quasiparticle and phonon distributions for a number of widely-used low transition temperature thin-film superconductors under constant, uniform illumination by sub-gap probe and pair-breaking signal photons simultaneously. From these distributions we calculate material-characteristic parameters that allow rapid evaluation of an effective quasiparticle temperature using a simple analytical expression, for all materials studied (Mo, Al, Ta, Nb, and NbN) for all photon energies. We also explore the temperature and energy-dependence of the low-energy quasiparticle generation efficiency η by pair-breaking signal photons finding $\eta \approx 0.6$ in the limit of thick films at low bath temperatures that is material-independent. Taking the energy distribution of excess quasiparticles into account, we find $\eta \rightarrow 1$ as the bath temperature approaches the transition temperature in agreement with the assumption of the two-temperature model of the nonequilibrium response that is appropriate in that regime. The behaviour of η with signal frequency scaled by the superconducting energy gap is also shown to be material-independent, and is in qualitative agreement with recent experimental results. An enhancement of η in the presence of sub-gap (probe) photons is shown to be most significant at signal frequencies near the superconducting gap frequency and arises due to multiple photon absorption events that increase the average energy of excess quasiparticles above that in the absence of the probe.

PACS numbers: 74.40.Gh, 74.78.-w, 29.40.-n, 74.25.N-

I. INTRODUCTION

The energy distribution of the quasiparticle excitations of a superconductor determines its electrical¹ and thermal transport properties.² A theoretical understanding of devices including kinetic inductance detectors (KIDs),³⁻⁵ superconducting tunnel junctions,⁶ superconducting qubits,⁷⁻⁹ SQUID based parametric amplifiers and mixers,¹⁰ and quantum capacitance detectors¹¹ requires a description of the quasiparticle system response. Therefore, a method for calculating the excited, possibly nonequilibrium distribution of quasiparticles is central to any device model.

Nonequilibrium superconducting detectors rely on pair-breaking to create their detected signal. We are particularly interested in thin-film superconductors fabricated on a dielectric substrate that is cooled to a sufficiently low temperature (the bath temperature) T_b . Typically $T_b \sim 0.1 T_c$ where T_c is the superconducting transition temperature. An interacting signal photon of energy $h\nu_{\text{signal}}$, where h is Planck's constant and ν_{signal} the signal frequency, directly breaks a condensate pair in the superconductor provided $h\nu_{\text{signal}} \geq 2\Delta$ where Δ is the superconducting energy gap. Due to the high density of states close to the gap, and for moderate energy photons, the interaction creates a distribution of excited quasiparticles with peaks¹² at $E = \Delta$ and $E = h\nu_{\text{signal}} - \Delta$ where E is the quasiparticle energy. E is related to the underlying Bloch state energy ϵ by $E = \sqrt{\epsilon^2 + \Delta^2}$. Higher energy signal photons will directly release an atomic electron via the photoelectric effect. In this case effects associated with localized heating and gap-reduction or "hotspots"

may become important. In this work we concentrate on modelling the detection of moderate energy photons $h\nu_{\text{signal}} < \Omega_D$ where these effects are insignificant. The photon energies considered are particularly important to understand the responsivity, sensitivity and signal-to-noise of currently-deployed and planned astronomical instruments performing measurements in the frequency window of 0.1 to 10 THz. In the case of KIDs, the nonequilibrium state created by the interaction is monitored using a probe of energy $h\nu_{\text{probe}} \ll 2\Delta$, where ν_{probe} is the probe frequency, so an additional drive term needs to be included in the detailed analysis.

An important consideration in any nonequilibrium superconducting detector operating at low reduced temperatures $T_b/T_c \ll 1$ is that the detected signal is most influenced by the presence of *low-energy* quasiparticles because the relaxation of the primary excitation occurs on time-scales that are much shorter than the ultimate relaxation time of the low-energy excess. (Here we define low-energy quasiparticles to have $E < 3\Delta$.) We assume the signal photons interact with 100% efficiency i.e. we ignore for example any optical coupling efficiencies. A primary excitation with $E = h\nu_{\text{signal}} - \Delta$ relaxes towards the gap emitting a phonon. If this emitted phonon has energy $\Omega \geq 2\Delta$, an additional pair may be broken enhancing the number of low-energy excess quasiparticles and thus the detected signal. But in a thin-film this emitted phonon may be lost into the substrate, reducing the number of low-energy excitations. The average number m of low-energy quasiparticles resulting from the interaction of a single high-energy photon can be quantified in terms of a quasiparticle generation efficiency (or quasiparticle yield) η . If the low-energy quasiparticles have average energy

$\langle E_{qp} \rangle$) then the efficiency $\eta = m\langle E_{qp} \rangle / h\nu_{\text{signal}}$. Often it is assumed $\langle E_{qp} \rangle = \Delta$.¹³

Phonon loss means $\eta \leq 1$. Most existing work assumes a value of $\eta \approx 0.6$ for all materials, photon frequencies and bath temperatures.³ At high temperatures $T \approx T_c$ our description of the energy-cascade no longer applies^{14,15} because thermal phonon energies become comparable with Δ , and scattering and recombination occur on comparable timescales. Then a two-temperature model describing the quasiparticle and phonon systems that assumes $\eta = 1$ is most appropriate. Here we show that the full nonequilibrium calculation yields $\eta \rightarrow 1$ as $T_b/T_c \rightarrow 1$ in agreement with the assumption of the two-temperature model.

Previous work modelled the effect of incoming energy at low temperatures with an effective temperature¹⁶ or as an effective chemical potential¹⁷ for the quasiparticle distribution. To go beyond this analysis, Chang and Scalapino^{18,19} derived a set of coupled nonlinear kinetic equations describing the interactions of quasiparticles and phonons to find their respective energy distributions $f(E)$ and $n(\Omega)$. They solved for the nonequilibrium distributions resulting from various drive terms, including photon and phonon injection. A number of investigations have explored the effect of very high energy photons (x-ray or optical photons) on infinite superconductors^{20,21} and thin films²² calculating a quasiparticle generation efficiency of $\eta \approx 0.6$, ignoring $\Omega \geq 2\Delta$ phonon loss. Another approach¹³ considered the time-evolution following local energy deposition into the thin film. Kozorezov *et al.*²³ considered the energy downconversion process after absorption of a high energy photon for a variety of materials and concluded that the materials can be categorized into three different classes, with the low energy-gap superconductors all having $\eta \approx 0.6$.

We have previously reported²⁴ a numerical approach that solves the coupled kinetic equations describing the quasiparticle and phonon distributions $f(E)$ and $n(\Omega)$ for a superconducting thin-film driven by a sub-gap probe,²⁴ and including the effect of an additional pair-breaking signal,²⁵ for Al thin-films at low temperatures $T \sim 0.1 T_c$. We have also reported detailed calculations of KID characteristics (quality factors and quasiparticle lifetimes as functions of readout power and T_b) that were compared to precise measurements of Al resonator behaviour finding good agreement.²⁶ More recent measurements on KIDs²⁷ of the quasiparticle number and recombination time-dependence on readout power appear to show that they must be explained using nonequilibrium quasiparticle distributions. Other recent measurements with a Ta KID²⁸ report a detector response that has the same qualitative features as the energy dependence of η for Al described in Guruswamy *et al.*²⁵ Here we apply the method to a number of other technologically important low temperature superconductors and discuss the physics involved. We concentrate in particular on the refractory elements and extend the earlier analysis to bath temperatures approaching the superconducting critical temperature T_c . We study Mo, Al, Ta (in its higher $T_c \sim 4.4$ K form), Nb and NbN. In

each instance we use measured material properties that characterize films that we deposit by sputtering under ultra-high-vacuum. Our results are applicable to many different device designs, as only the phonon escape time to the substrate τ_i is device-geometry dependent. The method assumes that phonon pair-breaking, quasiparticle recombination, and electron-phonon scattering are the only significant interaction processes. This assumption is investigated in section II B for typical thin-films intended for detector applications. Section II reviews superconducting parameters for the materials discussed, considers the relative contribution from electron-electron scattering for the different materials, describes the numerical method, and also describes how η is calculated for a pair-breaking signal. Section III presents an analytical superconductor cooling model that can be used to calculate the effective quasiparticle temperature T_N^* for both sub-gap and pair-breaking photons. Section IV describes detailed numerical results for both sub-gap and pair-breaking photon interactions including the effect of the effect of changes in the bath temperature. Section V summarizes the work done.

II. METHODS

A. Superconducting parameters

The superconducting parameters needed for modelling are the characteristic quasiparticle lifetime

$$\tau_0 = \frac{Z_1(0)\hbar}{2\pi b(k_B T_c)^3}, \quad (1)$$

and the characteristic phonon lifetime

$$\tau_0^\phi = \frac{\hbar N_{\text{ion}}}{4\pi^2 N(0)_{\text{bs}} \langle \alpha^2 \rangle \Delta_0}, \quad (2)$$

as defined by Kaplan *et al.*²⁹ $N(0)$ and $N(0)_{\text{bs}}$ are the mass-enhanced and bare single-spin density of states at the Fermi energy ϵ_F respectively, where $N(0) = Z_1(0)N(0)_{\text{bs}}$, N_{ion} is the ion density, and Δ_0 the zero temperature superconducting energy gap. $Z_1(0)$ is the electron-phonon renormalization factor $Z_1(0) = 1 + \lambda$, where $\lambda = 2 \int_0^\infty d\Omega \alpha^2(\Omega)F(\Omega)/\Omega$ is the dimensionless electron-phonon coupling strength. $\alpha^2(\Omega)F(\Omega)$ is the Eliashberg function, $\alpha^2(\Omega)$ is the electron-phonon interaction matrix element and $F(\Omega)$ is the phonon density of states. The material-dependent parameter b is calculated within a Debye model such that $b\Omega^2 = \alpha^2(\Omega)F(\Omega)$ for low phonon energies $\Omega \sim 2\Delta_0$. The averaged value of the interaction matrix element is $\langle \alpha^2 \rangle = 1/3 \int_0^\infty d\Omega \alpha^2(\Omega)F(\Omega)$. Values of b and $\langle \alpha^2 \rangle$ for Al, Ta and Nb are already tabulated.²⁹ For Mo we use the point-contact measurements of Caro *et al.*³⁰ while for NbN we use the tunnelling data of Kihlstrom *et al.*³¹ and the transport property measurements of Semenov *et al.*³² We note that the precision of our calculations of b are dependent on the accuracy

within which we can interpret the relevant low-frequency parts of the reported $\alpha^2(\Omega)F(\Omega)$ data.

Material	Mo	Al	Ta	Nb	NbN
Δ_0 (μeV)	140	180	700	1470	2560
ν_{gap} (GHz)	68	87	339	711	1240
T_c/K	0.92	1.18	4.6	9.67	16.8
b (10^{-4}meV^{-2})	2.28	3.17	17.3	40	47
$\langle\alpha^2\rangle$ (meV)	1.62	1.93	1.38	4.6	4.99
λ	0.42	0.43	0.69	1.84	1.46
τ_0 (ns)	1310	438	1.78	0.15	0.02
τ_0^ϕ (ps)	231	260	22.7	4.17	5.98
$\tau_{\text{ec}}^\phi/\tau_0^\phi$	1.04	1.04	0.91	0.94	1.01

Table I. Characteristic quasiparticle and phonon lifetimes, and associated parameters. Data from Gladstone *et al.*³³, Kaplan *et al.*²⁹ or Zehnder¹³ unless otherwise specified. For Mo and NbN we use measurements of $\alpha^2(\Omega)F(\Omega)$ from Caro *et al.*³⁰ and Kihlstrom *et al.*³¹ respectively. τ_{ec}^ϕ is the value of τ_0^ϕ required for energy conservation calculated from (8). $\nu_{\text{gap}} = 2\Delta_0/h$ is the gap frequency.

The characteristic times calculated are listed in table I. We assume the weak-coupling relationship $\Delta_0 = 1.76 k_B T_c$ for all materials to determine T_c in table I. The assumption is reasonable for Mo Al and Ta, but gives a slightly higher T_c compared to experiment for Nb (typically $T_c \sim 9.3\text{K}$) and for NbN ($T_c \sim 15\text{K}$). However we do not expect the assumption to significantly affect the physics of the conclusions drawn; the differences introduced by strong coupling are reduced because of the short lifetimes of states with energy $E \gg \Delta$.^{18,29} τ_{ec}^ϕ is the value of τ_0^ϕ required for energy conservation calculated from (8) and discussed in more detail in section II C.

B. Electron-electron vs electron-phonon scattering

Insight into the contribution from electron-electron $e-e$ scattering in the down-conversion process is most-easily found by considering the relevant scattering rates T_c . For the electron energies of interest $\epsilon \ll \Omega_D$, we assume that electron-phonon ($e-p$) inelastic scattering dominates over ($e-e$) scattering. We previously investigated²⁵ to what extent this assumption is valid for low-resistivity Al films. Now we consider the other low- T_c superconductors using material parameters typical of those that we measure experimentally for the thin-films we deposit by magnetron-sputtering in ultra-high vacuum.

In the normal-state the $e-p$ scattering rate τ_{e-p}^{-1} is³⁴

$$\tau_{e-p}^{-1}(\epsilon) = \frac{2\pi}{\hbar} \int_0^\epsilon d\Omega \alpha^2(\Omega)F(\Omega). \quad (3)$$

Assuming $\alpha^2(\Omega)$ is constant at low energies, a Debye

model for phonons²⁹ leads to

$$\tau_{e-p}^{-1}(\epsilon) = \begin{cases} \frac{\epsilon^3}{3\tau_0(k_B T_c)^3} & \text{if } \epsilon < \Omega_D \\ \frac{\Omega_D^3}{3\tau_0(k_B T_c)^3} & \text{if } \epsilon \geq \Omega_D \end{cases}. \quad (4)$$

The electron-electron scattering rate in clean films is estimated with the Landau-Pomeranchuk formula²³

$$\tau_{e-e}^{-1}(\epsilon) = \frac{\epsilon^2}{\hbar\epsilon_F} \frac{r_s^{1/2}}{7.96}, \quad (5)$$

where r_s is the radius containing one electron charge divided by the Bohr radius (approximated as 1). For thin resistive films the $e-e$ rate can be significantly enhanced so that³⁵

$$\tau_{e-e}^{-1}(\epsilon, R_{sq}) = \frac{e^2 R_{sq} \epsilon}{2\pi^2 \hbar^2} \ln^{-1} \frac{\hbar\pi}{e^2 R_{sq}}, \quad (6)$$

where $R_{sq} = \rho/d$ is the sheet resistance of the thin-film, ρ is the resistivity and d is the thickness.³⁶ These normal-state calculations significantly overestimate the $e-e$ scattering rates in the superconducting state at low temperatures $T_b \ll T_c$.³⁷ Figure 1 plots the normal-state scattering rates for a 40 nm thick Mo film and we have used the thin-film resistive $e-e$ scattering rate (6). We identify

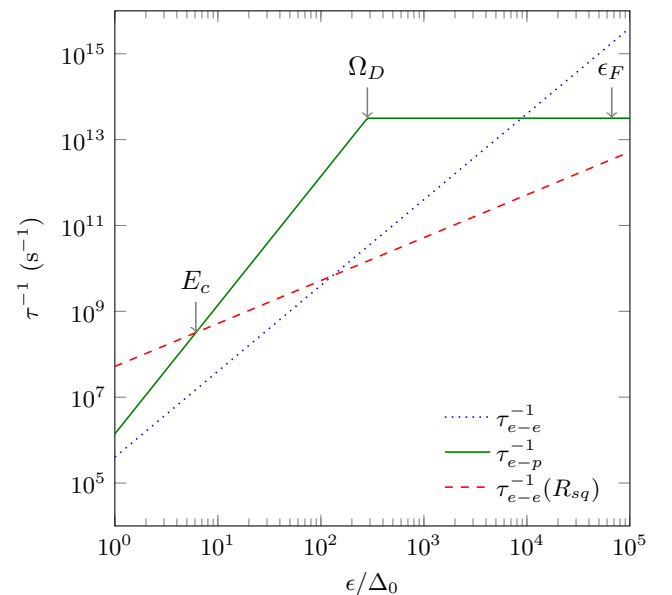


Figure 1. Energy dependence of normal state scattering rates in Mo. Electron-phonon rate $\tau_{e-p}^{-1}(\epsilon)$ (solid green), clean limit electron-electron rate $\tau_{e-e}^{-1}(\epsilon)$ (dotted blue), and thin-film resistive $\tau_{e-e}^{-1}(\epsilon, R_{sq})$ (dashed red). Calculations are for a 40 nm Mo film with $\rho = 9.2 \times 10^{-8} \Omega\text{m}$.

the following characteristic energies for each material: ϵ_F ; Ω_D ; and a low-energy crossover E_c , below which the $e-e$ scattering rate exceeds the $e-p$ rate. E_c/Δ is highest

Material	ρ ($10^{-8}\Omega\text{m}$)	d (nm)	ϵ_F (eV)	Ω_D (meV)	E_c/Δ_0
Mo	9.2	40	9.32	39.6	6.1
Al ³⁸	0.8	35	11.6	36.2	1.42
Ta (bcc, epi)	4.1	100	9.5	20.7	0.23
Nb	8.8	100	6.18	23.7	0.14
NbN ^{39,40}	250	100	15.6	28.4	0.3

Table II. Characteristic material energies related to scattering. E_c is the energy at which the electron-phonon scattering rate becomes greater than the thin-film resistive electron-electron scattering rate. Data from Gladstone *et al.*³³, Kaplan *et al.*²⁹ or Kozorezov *et al.*²³ unless otherwise referenced. The material resistivities and thicknesses used are measured values from thin-films deposited by our group. All data is for polycrystalline films except for Ta where we assume parameters typical of the higher- T_c bcc form.

for Mo for the material parameters chosen, as shown in table II.

During the energy down-conversion, the inelastic scattering rate is only relevant above energies $E \geq 3\Delta$ where additional pair breaking is possible. We find that E_c is below 3Δ for all materials except Mo. Figure 1 shows that $e-p$ scattering dominates in that case for $\epsilon \approx 6\Delta$ to $10^4\Delta$ for the modelled Mo film, and $e-e$ scattering may contribute above and below this energy range. However, the $e-e$ scattering rate is considerably suppressed in the superconducting state at low T/T_c .³⁷ We conclude that there is negligible contribution from $e-e$ scattering for most of these materials, thicknesses, temperatures and signal photon energies. For Mo we note that additional $e-e$ scattering may increase the quasiparticle generation efficiency over the results presented here by providing an additional pair-breaking mechanism especially near T_c .

C. Numerical method

We solved the coupled kinetic equations¹⁸ describing the quasiparticle and phonon distributions numerically to find the steady-state driven distributions, $f(E)$ $n(\Omega)$ for the quasiparticles and phonons respectively, using Newton-Raphson iteration. Drive terms for pair-breaking and sub-gap photons⁴¹ were included as necessary and the numeric pre-factors of these terms scaled to match the absorbed powers, P_{probe} for sub-gap photons and P_{signal} for the pair-breaking signal. The numerical method was iterated until the solutions conserved energy to within $\xi = 10^{-5}$. This was quantified as $\xi = \sqrt{\xi_{qp-\phi}^2 + \xi_{\phi-b}^2}$, where $\xi_{qp-\phi}$ is the relative difference between the photon power absorbed and power flow from quasiparticles to phonons, and $\xi_{\phi-b}$ is the relative difference between the photon power absorbed and the power flow from phonons to substrate (held at a temperature T_b). The numerical method is outlined in more detail in Goldie and Withington.²⁴

For each material, the temperature dependent energy

gap $\Delta(T)$ was calculated using the BCS gap equation,

$$\frac{1}{N(0)V_{\text{BCS}}} = \int_{\Delta(T)}^{\Omega_D} dE \frac{1 - 2f(E, T)}{\sqrt{E^2 - \Delta(T)^2}}, \quad (7)$$

where $f(E, T) = (\exp(E/k_B T) + 1)^{-1}$ is the Fermi-Dirac distribution, and $N(0)V_{\text{BCS}}$ is the dimensionless electron-phonon coupling constant, calculated from the zero temperature form of (7) as $N(0)V_{\text{BCS}} = 1/\sinh^{-1}(\Omega_D/\Delta_0)$.

The numerical method converges on a solution that minimizes ξ provided the material parameters satisfy

$$\frac{2\pi N(0)\tau_0^\phi \Delta_0 \Omega_D^3}{9N_{\text{ion}}\tau_0(k_B T_c)^3} = 1, \quad (8)$$

a consequence of matching the low energy part of the measured Eliashberg function to a Debye-model approximation that determines b . In our previous work we ensured that T_c satisfied (8),²⁴ but then the T_c obtained did not precisely agree with (7) (although the difference is small $< 1\%$). In this work, since we are also interested in the temperature dependence of the response we calculated T_c from (7) and defined an energy-conserving characteristic phonon lifetime τ_{ec}^ϕ to satisfy (8). Given the difficulty of interpreting the low-energy $\alpha^2(\Omega)F(\Omega)$ data that we and indeed Kaplan *et al.*²⁹ and others have noted we consider this approach entirely reasonable. The ratios $\tau_{\text{ec}}^\phi/\tau_0^\phi$ are given in table I. Satisfyingly the ratios are within 10% of unity for all materials studied. In our calculation of b for Mo, our error would be of this order given the difficulty of determining the low-energy $\alpha^2(\Omega)F(\Omega)$ from the available data. We note that other estimates of the characteristic times exist (see for example Parlato *et al.*⁴²) although those estimates do not necessarily satisfy the energy-conserving requirement.

In the numerical code the energy-bin distribution for both the quasiparticles and phonons was also changed when calculating bath temperature dependencies. As T_b is increased, the phonon-bath power flow $P(\Omega)_{\phi-b}$ above $\Omega = 2\Delta$ increasingly resembles the difference between two thermal distributions, and an increasing fraction of power is carried by high energy phonons, as shown in figure 2. Therefore at high temperatures, the phonon distribution must be accurately calculated to these higher energies. The energy of the last phonon bin Ω_{max} significantly affects the energy conservation of the solutions. Figure 2 (inset) shows that to have a relative power flow difference $\xi_{\phi-b} < 10^{-5}$, required $\Omega_{\text{max}} > 15k_B T_b$ for $T_b/T_c = 0.95$.

However, the bin width could not be made too large as the energy gap $\Delta(T)$, readout photon energy $h\nu_p$, and signal photon energy $h\nu_s$ had to be rounded to the nearest multiple of the bin width, such that the photon-induced peaks in the distributions occurred within well-defined energy bins. We chose to model the phonons with $N = 2500$ uniformly-sized bins with maximum phonon energy Ω_{max} , and similarly the quasiparticles with maximum energy $E_{\text{max}} = \Omega_{\text{max}} + \Delta(T)$. Bin width was therefore variable,

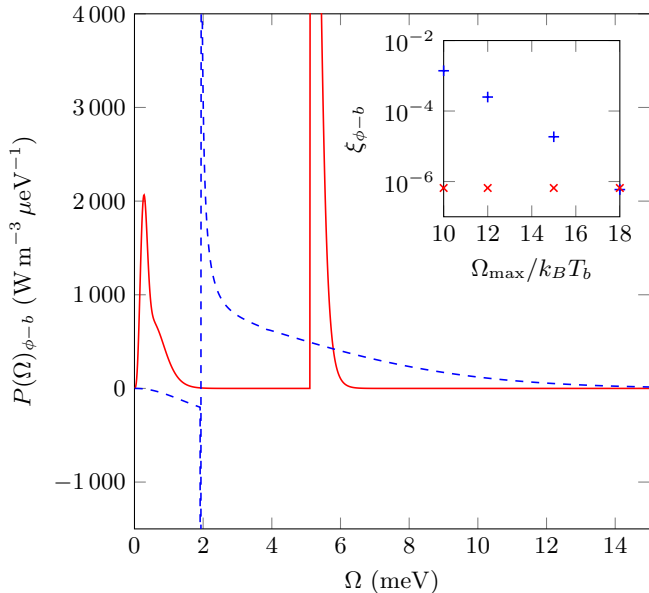


Figure 2. Phonon-bath power flow $P(\Omega)_{\phi-b}$, at $T_b = 0.1 T_c$ (solid red) and $T_b = 0.95 T_c$ (dashed blue). Both for NbN, $P_{\text{probe}} = 2 \times 10^6 \text{ W m}^{-3}$, $P_{\text{signal}} = 0$, $\tau_l/\tau_0^\phi = 1$, and $h\nu_{\text{probe}} = 16 \mu\text{eV}$. Inset of relative phonon-bath power flow difference $\xi_{\phi-b}$ against the energy of the maximum bin $\Omega_{\text{max}}/k_B T_b$, at the same bath temperatures $T_b = 0.1 T_c$ (red \times) and $T_b = 0.95 T_c$ (blue $+$).

depending on material and temperature. The quasiparticle density of states broadening parameter γ was recalculated for each simulation, changing for different material and bin width combinations. It was chosen to minimize the difference between the quasiparticle number calculated as the integral $4N(0) \int_{\Delta}^{\infty} dE \rho_{\text{BCS}}(E, \Delta) f(E, T_b)$, where $\rho_{\text{BCS}}(E, \Delta) = E/\sqrt{E^2 - \Delta^2}$, and the equivalent sum over the discretized distribution with the broadened density of states calculated with $E \rightarrow E + i\gamma$. In all cases the approach worked well.

D. Low-energy quasiparticle generation efficiency for a pair-breaking signal

For a single pair-breaking photon we have defined a low-energy generation efficiency $\eta = m\langle E_{qp} \rangle / h\nu_{\text{signal}}$. Here we describe the calculation of η for a constant input signal power P_{signal} in a thin-film that may also be driven by a non-direct pair-breaking constant readout power P_{probe} (such as used for KID readout). The absorbed power creates a number of excess quasiparticles $N_{\text{excess}} = N_{\text{signal}} - N_{\text{probe}}$ such that the quasiparticle system total energy has increased by $E_{\text{excess}} = E_{\text{signal}} - E_{\text{probe}}$, where N_{signal} and E_{signal} are the quantities for distributions driven by the signal and probe together. In the steady state, photons absorbed at a rate Γ_ϕ create low-energy quasiparticles at a rate $\Gamma_{qp} = m\Gamma_\phi$.

Solving a modified set of Rothwarf-Taylor rate equa-

tions⁴³ for Γ_ϕ and Γ_{qp} results in²⁵

$$\eta = \langle E_{qp} \rangle \frac{(N_{\text{signal}}^2 - N_{\text{probe}}^2)}{P_{\text{signal}}} \frac{2R}{1 + \beta\tau_l}, \quad (9)$$

where R and β are the distribution-averaged recombination rate and pair-breaking rates respectively. We define $\langle E_{qp} \rangle$ the average energy of the excess low-energy quasiparticles where

$$\langle E_{qp} \rangle = \frac{\int_0^\infty E \rho(E) (f(E) - f(E, T)) dE}{\int_0^\infty \rho(E) (f(E) - f(E, T)) dE}. \quad (10)$$

At low temperatures $\langle E_{qp} \rangle \approx \Delta$ as usually assumed: taking account of the detailed energy distributions allows η to be determined at arbitrary temperatures.

III. SUPERCONDUCTOR COOLING MODEL

We used the steady-state driven distributions that were calculated to determine parameters for the thin-film superconductor cooling model outlined in Goldie and Withington.²⁴ This model is an analytic expression relating T_N^* to the power flow P between the quasiparticle and phonon systems (the latter assumed to be the substrate phonons) for a given $T_b \ll T_c$ and material.

$$P = \frac{1}{\eta(P, \nu)} \frac{\Sigma_s}{1 + \tau_l/\tau_{pb}} \times \left[T_N^* \exp\left(\frac{-2\Delta(T_N^*)}{k_B T_N^*}\right) - T_b \exp\left(\frac{-2\Delta(T_b)}{k_B T_b}\right) \right]. \quad (11)$$

Σ_s is a material-dependent constant, τ_{pb} is the phonon pair breaking time, $\sim \tau_0^\phi$ for $T_b \ll T_c$. T_N^* is the effective temperature calculated to characterize the driven nonequilibrium quasiparticle distributions so that $N_{qp} = 4N(0) \int_{\Delta}^{\infty} dE \rho(E) f(E, T_N^*)$. $\eta(P, \nu)$ depends on the drive (probe or pair-breaking signal). Goldie and Withington²⁴ showed for a sub-gap probe $\eta(P, \nu_{\text{probe}}) \equiv \eta_{2\Delta}$ the fraction of phonon-bath power flow carried by excess phonons with energy $\Omega > 2\Delta(T_b)$ that depends on P , ν_{probe} and τ_l . Here we show that (11) can also be applied for direct pair-breaking when $\eta(P, \nu_{\text{signal}}) \equiv \eta$ as defined in section II D.

IV. RESULTS

A. Effects of a sub-gap probe

Here we show and discuss results for modelling of the effect of a sub-gap probe. The data-points (crosses) in figure 3(a) show the calculated T_N^* from the full non-equilibrium solution as a function of P_{probe} . The solid line shows T_N^* evaluated with (11) and from this

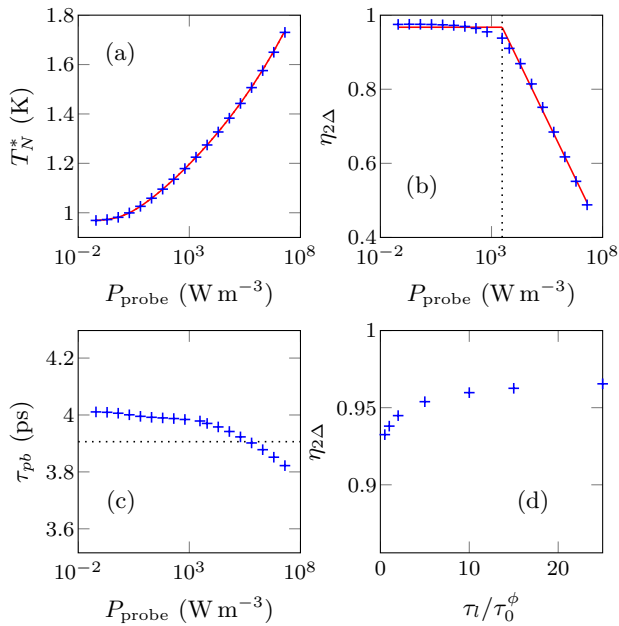


Figure 3. (a) Effective quasiparticle temperatures T_N^* as a function of P_{probe} ; full nonequilibrium calculation (blue +), and a fit using (11) (red solid line). (b) Fraction of phonon-bath power flow carried by $\Omega > 2\Delta$ excess phonons as a function of P_{probe} ; full nonequilibrium calculation (blue +), and piecewise fit (red line) to (12). The dotted vertical line marks P_0 . (c) Distribution-averaged phonon pair-breaking time τ_{pb} . The characteristic phonon lifetime τ_0^ϕ is marked with the dotted line. (d) $\eta_{2\Delta}$ as a function of phonon escape time ratio τ_l/τ_0^ϕ . The calculations are for Nb, with $P_{\text{probe}} = 2 \times 10^3 \text{ W m}^{-3}$, $h\nu_{\text{probe}} = 16 \mu\text{eV}$, and $\tau_l/\tau_0^\phi = 1$.

we also calculate Σ_s . The calculations are for Nb, with $P_{\text{probe}} = 2 \times 10^3 \text{ W m}^{-3}$, $h\nu_{\text{probe}} = 16 \mu\text{eV}$, and $\tau_l/\tau_0^\phi = 1$. The analytical model is an excellent approximation to the full nonequilibrium calculation provided the power-dependence of $\eta_{2\Delta}$ shown in figure 3(b) is taken into account. The solid line in figure 3(b) is a piecewise fit such that

$$\eta_{2\Delta}(P) = \begin{cases} \eta_0 & \text{if } P \leq P_0 \\ \eta_1 \ln(P/P_0) + \eta_0 & \text{if } P > P_0. \end{cases} \quad (12)$$

P_0 characterizes a “knee” probe power below which $\eta_{2\Delta}$ is constant and η_1 characterizes the energy dependence of $\eta_{2\Delta}$ at higher probe powers. Both are material dependent. Figure 3(c) shows that $\tau_{pb} \sim \tau_0^\phi$ is a good approximation over the range of interest. Figure 3(d) shows that $\eta_{2\Delta}$ has no significant dependence on the phonon escape time τ_l .

The dependence of the fit parameters P_0 , η_0 , and η_1 on probe photon energy is shown in figure 4. This includes calculations for Nb (blue \times), Ta (green \square), and Al (red \circ). Scaling the energy of the photon by Δ_0 demonstrates the monotonic behaviour for all the materials. P_0 shown in figure 4(a) is scaled by the material-dependent Σ_s to

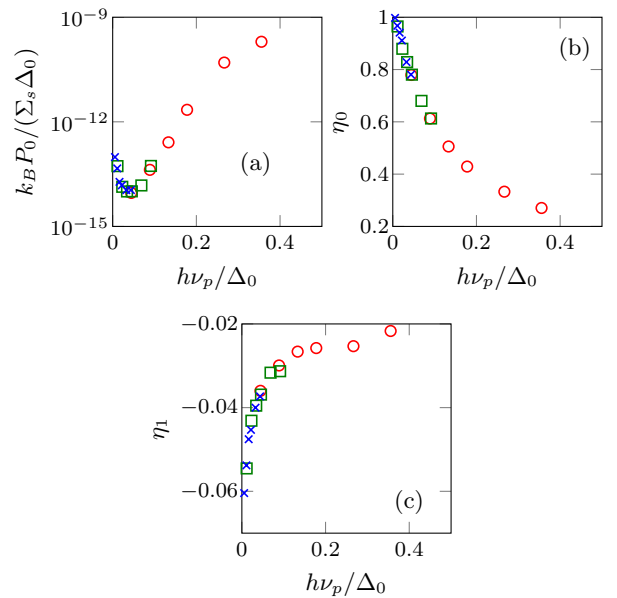


Figure 4. Parameters for piecewise fits to $\eta_{2\Delta}$ for Nb (blue \times), Ta (green \square), and Al (red \circ) calculated at a range of frequencies $h\nu_{\text{probe}}$. (a) P_0 against scaled frequency. (b) η_0 (constant section) against scaled frequency. (c) η_1 (slope for linear section) against scaled frequency.

emphasize the commonality.

Material	Δ_0 (μeV)	Σ_s ($\text{W m}^{-3} \text{ K}^{-1}$)	P_0 (W m^{-3})
Mo	140	$1.42 \cdot 10^{10}$	$2.96 \cdot 10^{-3}$
Al	180	$3.23 \cdot 10^{10}$	$2.83 \cdot 10^{-3}$
Ta	700	$1.17 \cdot 10^{14}$	$1.30 \cdot 10^1$
Nb	1470	$3.83 \cdot 10^{15}$	$3.02 \cdot 10^3$
NbN	2560	$1.29 \cdot 10^{16}$	$3.17 \cdot 10^4$

Table III. Superconductor cooling model material parameter Σ_s , and knee power P_0 at $h\nu_{\text{probe}} = 16 \mu\text{eV}$ and $\tau_l/\tau_0^\phi = 1$, obtained from fits to results of the full nonequilibrium calculation.

Table III summarizes parameters derived from the modelling to describe sub-gap photon interactions in all of the materials studied. The table shows Σ_s and knee parameter P_0 at $h\nu_{\text{probe}} = 16 \mu\text{eV}$ and $\tau_l/\tau_0^\phi = 1$. The values of Σ_s shown can also be used for estimates of T_N^* for a direct pair-breaking signal as we will discuss in the next section with an appropriate energy-dependent η .

B. Effects of direct pair-breaking

Here we discuss results for a direct pair-breaking signal with $2\Delta < h\nu_{\text{signal}} < 10\Delta$. Figure 5 shows how η varies with signal photon energy. η decreases from unity in the range $h\nu_{\text{signal}} = 2\Delta$ to 4Δ , as phonons emitted by quasiparticles scattering towards the gap escape the

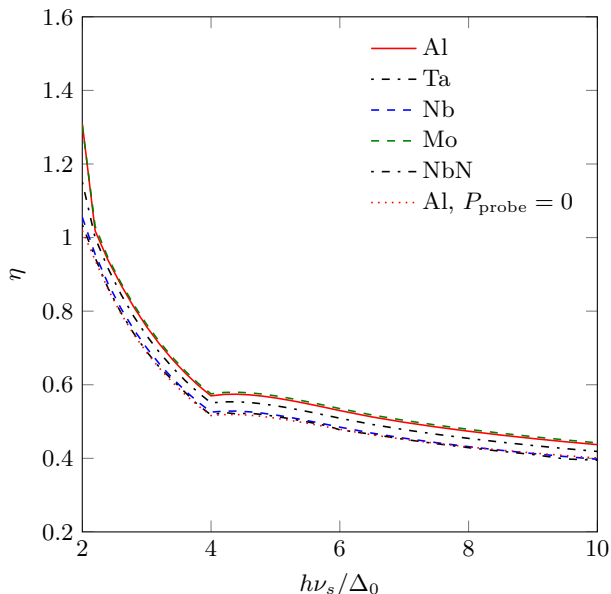


Figure 5. Quasiparticle generation efficiency η_{power} against signal photon energy $h\nu_{\text{signal}}$ for different materials. Calculated for $T_b = 0.1T_c$, $P_{\text{probe}} = 2 \times 10^3 \text{ W m}^{-3}$, $h\nu_{\text{probe}} = 16 \mu\text{eV}$, $P_{\text{signal}} = 2 \text{ W m}^{-3}$, and $\tau_l/\tau_0^\phi = 1$.

thin film. Above $h\nu_{\text{signal}} = 4\Delta$, the phonons emitted in scattering can break additional Cooper pairs, increasing the quasiparticle generation efficiency. The magnitude of the increase depends on the phonon trapping factor.²⁵ Measurements of the response of a Ta KID²⁸ at signal frequencies close to the gap energy show these characteristic features. The figure shows that when $h\nu_{\text{signal}}$, T_b and τ_l are scaled by the relevant material parameters, the quasiparticle generation efficiency is the same for all materials. Kozorezov *et al.*²³ predicted that the quasiparticle generation efficiency could be categorized into three classes of superconductors. The superconductors included in this work, which fall within either the second (Ta, Nb, NbN) or third (Al, Mo) class, have a material-independent $\eta \approx 0.6$. This conclusion differs somewhat from that of Zehnder.¹³ We understand this as due to the current work examining the steady-state response to constant incoming power, and scaling all relevant parameters by material characteristics, whereas Zehnder's work examined the time-dependent response including quasiparticle out-diffusion from a localized hot-spot, and chose a fixed cutoff time of 10 ns to calculate the quasiparticle generation efficiency unscaled by material. We emphasize that for the low energy photons considered in the present work localized hot-spot formation (and consequent gap suppression) does not occur for the signal powers studied.

The other effect shown in figure 5 is the enhancement of η by the readout power due to an increase in the average energy of generated quasiparticles. For $h\nu_{\text{signal}} \simeq 2\Delta$, it can be seen that $\eta > 1$ which may seem unreasonable. The enhancement is due to multiple photon absorption by the quasiparticles i.e. both signal and probe, and

the effect is most-pronounced near $h\nu_{\text{signal}} = 2\Delta$. This results in a higher average excess quasiparticle energy when the readout power is present alongside the signal compared to when only the signal is present, and also produces the small variation in η between materials. The absorbed readout power P_{probe} and readout frequency $h\nu_{\text{probe}}$ are not scaled by material parameters in this figure, unlike the signal. When calculated with $P_{\text{probe}} = 0$, the signal quasiparticle generation efficiency is identical for all materials and is unity at $h\nu_{\text{signal}} = 2\Delta$.

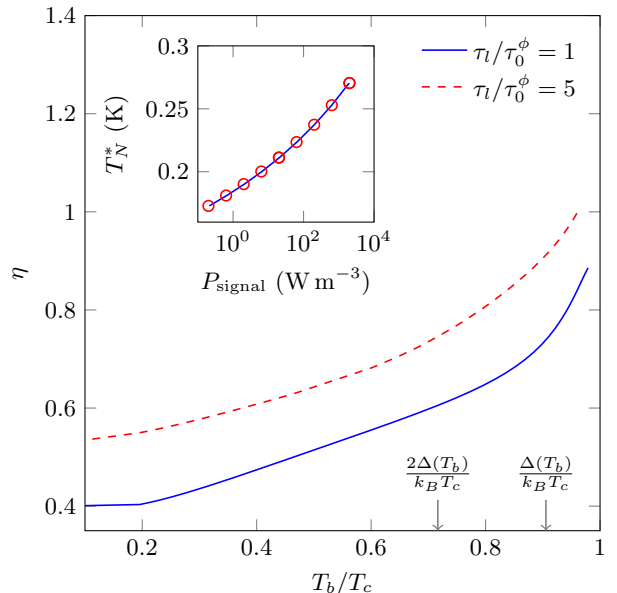


Figure 6. The quasiparticle generation efficiency η as a function of reduced temperature T_b/T_c . The calculation is for Al, with $P_{\text{probe}} = 0$, $P_{\text{signal}} = 2 \text{ W m}^{-3}$, $h\nu_{\text{signal}} = 10 \Delta(T_b)$, and two values of the phonon escape time. The inset shows T_N^* calculated using the full nonequilibrium model (red \circ) and using (11) (blue line) as a function of P_{signal} with $T_b = 0.1T_c$ and $\tau_l/\tau_0^\phi = 1$.

Figure 6 shows the variation in η as the bath temperature is changed. As T_b increases, the scattering between the more numerous thermal quasiparticles and phonons determines the structure of the driven distribution, rather than scattering between the excess quasiparticles and phonons. This means the power flow from phonons to bath does not have the same peaked structure and instead more closely resembles the difference between two thermal distributions, as earlier shown in figure 2. This type of excess quasiparticle distribution means the average energy of generated quasiparticles increases without increasing the recombination and pair breaking rates. The figure also indicates temperatures for which $k_B T_b = 2\Delta(T_b)$ and $= \Delta(T_b)$, above which we expect thermal and nonequilibrium distributions to interact strongly. As $T_b/T_c \rightarrow 1$ we see that $\eta \rightarrow 1$ in agreement with the two-temperature model valid in that regime. We find that T_N^* is well-accounted for by (11), with the value of η shown, for $T_b/T_c \leq 0.7$. The inset shows T_N^* calculated using (11)

for $\tau_l/\tau_0^\phi = 1$ as a function of P_{signal} with $T_b = 0.1 T_c$.

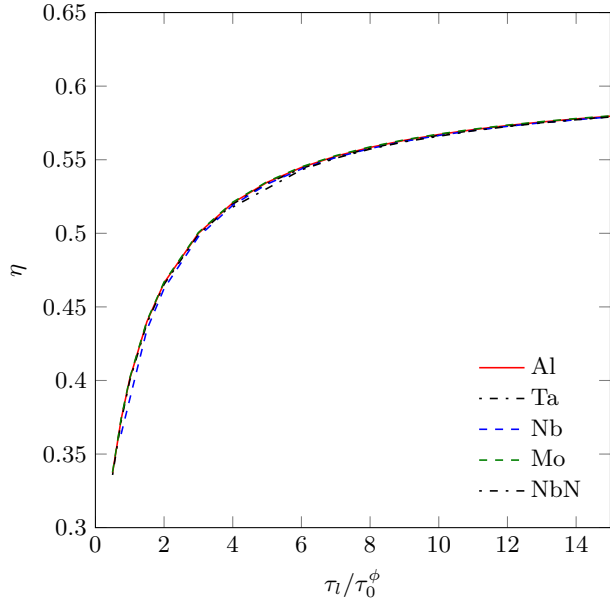


Figure 7. Quasiparticle generation efficiency η for materials studied as a function of phonon escape time τ_l/τ_0^ϕ . Calculation uses $T_b = 0.1 T_c$, $P_{\text{probe}} = 0$, $P_{\text{signal}} = 2 \text{ W m}^{-3}$, and $h\nu_{\text{signal}} = 10 \Delta$.

Figure 7 shows the dependence of η on the phonon trapping factor τ_l/τ_{pb} for $T_b = 0.1 T_c$. As the phonon escape time τ_l/τ_0^ϕ increases, the quasiparticle generation efficiency $\eta \rightarrow 0.6$ for all materials examined. This conclusion is in agreement with earlier Monte Carlo calculations^{20,22} for infinite superconductors or where $\Omega \geq 2\Delta$ phonon loss was ignored.

V. CONCLUSIONS

We have described solutions of the coupled kinetic equations that calculate steady-state nonequilibrium quasiparticle and phonon distributions in a number of technologically important superconducting thin-films driven by sub-gap and pair-breaking photons. In particular we consider low energy signal photon interactions $h\nu_{\text{signal}} \leq 10\Delta$, where localized heating and gap-suppression can be ignored. We have calculated numerical parameters for these superconductors that can be used in a simple analytical expression to describe the power-flow between quasiparticles and phonons. This expression allows straight-forward estimates of the effective quasiparticle temperatures for both sub-gap and pair-breaking drives to approximate the nonequilibrium behaviour without resorting to a full numeric solution of the coupled kinetic equations. The analytical expression is shown to give a good account of full solutions of the detailed equations for a wide range of powers and bath temperatures. This is relevant for predicting the behaviour of thin-film nonequilibrium superconducting detectors. We defined a low-energy quasiparticle generation efficiency for constant absorbed pair-breaking power and calculated detailed numerical solutions as a function of photon energies and bath temperature. We have shown that key parameters determining quasiparticle generation efficiency are the signal frequency and the phonon trapping factor. The enhancement of signal quasiparticle generation efficiency by absorbed readout power is demonstrated and explained as multiple-photon absorption (signal and probe) by the quasiparticles and Cooper pairs. We estimate this effect can result in an increase η of up to 20% at signal photon energies of $h\nu_{\text{signal}} = 2\Delta$. The most sensitive detectors currently in development may also be able to distinguish between phonon trapping factors using results presented here. For the low-energy photon interactions studied we also show that the quasiparticle generation efficiency is material independent.

* tg307@mrao.cam.ac.uk

¹ D. Mattis and J. Bardeen, Phys. Rev. **111**, 412 (1958).

² J. Bardeen, G. Rickayzen, and L. Tewordt, Phys. Rev. **113**, 982 (1959).

³ J. Zmuidzinas, Annu. Rev. Condens. Matter Phys. **3**, 169 (2012).

⁴ J. Baselmans, J. Low Temp. Phys. **167**, 292 (2012).

⁵ G. Vardoulakis, S. Withington, D. J. Goldie, and D. M. Glowacka, Meas. Sci. Technol. **19**, 015509 (2008).

⁶ S. Friedrich, J. Low Temp. Phys. **151**, 277 (2008).

⁷ L. DiCarlo, M. D. Reed, L. Sun, B. R. Johnson, J. M. Chow, J. M. Gambetta, L. Frunzio, S. M. Girvin, M. H. Devoret, and R. J. Schoelkopf, Nature **467**, 574 (2010).

⁸ M. Hofheinz, E. M. Weig, M. Ansmann, R. C. Bialczak, E. Lucero, M. Neeley, A. D. O'Connell, H. Wang, J. M. Martinis, and A. N. Cleland, Nature **454**, 310 (2008).

⁹ R. J. Schoelkopf and S. M. Girvin, Nature **451**, 664 (2008).

¹⁰ K. D. Irwin and K. W. Lehnert, Appl. Phys. Lett. **85**, 2107 (2004).

¹¹ J. Bueno, M. D. Shaw, P. K. Day, and P. M. Echternach, Appl. Phys. Lett. **96**, 103503 (2010).

¹² B. I. Ivlev, S. G. Lisitsyn, and G. M. Eliashberg, J. Low Temp. Phys. **10**, 449 (1973).

¹³ A. Zehnder, Phys. Rev. B **52**, 12858 (1995).

¹⁴ A. D. Semenov, G. N. Gol'tsman, and R. Sobolewski, Supercond. Sci. Technol. **15**, R1 (2002).

¹⁵ A. D. Semenov, R. S. Nebosis, Y. P. Gousev, M. A. Heusinger, and K. F. Renk, Phys. Rev. B **52**, 581 (1995).

¹⁶ W. Parker, Phys. Rev. B **12**, 3667 (1975).

¹⁷ C. Owen and D. Scalapino, Phys. Rev. Lett. **28**, 1559 (1972).

¹⁸ J.-J. Chang and D. J. Scalapino, Phys. Rev. B **15**, 2651 (1977).

- ¹⁹ J.-J. Chang and D. J. Scalapino, *J. Low Temp. Phys.* **31**, 1 (1978).
- ²⁰ M. Kurakado, *Nucl. Instrum. Methods* **196**, 275 (1982).
- ²¹ N. Rando, A. Peacock, A. van Dordrecht, C. Foden, R. Engelhardt, B. Taylor, P. Gare, J. Lumley, and C. Pereira, *Nucl. Instruments Methods* **313**, 173 (1992).
- ²² R. A. Hijmering, P. Verhoeve, D. D. E. Martin, A. G. Kozorezov, J. K. Wigmore, R. Venn, P. J. Groot, and I. Jerjen, *J. Appl. Phys.* **105**, 123906 (2009).
- ²³ A. G. Kozorezov, A. F. Volkov, J. K. Wigmore, A. Peacock, A. Poelaert, and R. den Hartog, *Phys. Rev. B* **61**, 11807 (2000).
- ²⁴ D. J. Goldie and S. Withington, *Supercond. Sci. Technol.* **26**, 015004 (2013).
- ²⁵ T. Guruswamy, D. J. Goldie, and S. Withington, *Supercond. Sci. Technol.* **27**, 055012 (2014), arXiv:1401.1937.
- ²⁶ P. J. de Visser, D. J. Goldie, P. Diener, S. Withington, J. J. A. Baselmans, and T. M. Klapwijk, *Phys. Rev. Lett.* **112**, 047004 (2014), arXiv:1306.4992.
- ²⁷ P. J. de Visser, J. J. A. Baselmans, J. Bueno, N. Llombart, and T. M. Klapwijk, *Nat. Commun.* **5**, 3130 (2014).
- ²⁸ A. Neto, N. Llombart, J. J. A. Baselmans, A. Baryshev, and S. J. C. Yates, *IEEE Trans. Terahertz Sci. Technol.* **4**, 26 (2014).
- ²⁹ S. Kaplan, C. Chi, D. Langenberg, J.-J. Chang, S. Jafarey, and D. Scalapino, *Phys. Rev. B* **14**, 4854 (1976).
- ³⁰ J. Caro, R. Coehoorn, and D. de Groot, *Solid State Commun.* **39**, 267 (1981).
- ³¹ K. Kihlstrom, R. Simon, and S. Wolf, *Phys. Rev. B* **32**, 1843 (1985).
- ³² A. Semenov, B. Günther, U. Böttger, H.-W. Hübers, H. Bartolf, A. Engel, A. Schilling, K. Ilin, M. Siegel, R. Schneider, D. Gerthsen, and N. Gippius, *Phys. Rev. B* **80**, 054510 (2009).
- ³³ G. Gladstone, M. Jensen, and J. Schrieffer, in *Superconductivity*, Vol. 2, edited by R. D. Parks (M. Dekker, New York, 1969) Chap. 13, p. 713.
- ³⁴ A. G. Kozorezov, *J. Low Temp. Phys.* **167**, 473 (2011).
- ³⁵ E. Gershenzon, G. Gol'tsman, V. Potapov, and A. Sergeev, *Solid State Commun.* **75**, 639 (1990).
- ³⁶ This differs by a factor of π from the expression given in Altshuler and Aronov⁴⁴.
- ³⁷ A. V. Sergeev and M. Yu. Reizer, *Int. J. Mod. Phys. B* **10**, 635 (1996).
- ³⁸ P. J. de Visser, J. J. A. Baselmans, S. J. C. Yates, P. Diener, A. Endo, and T. M. Klapwijk, *Appl. Phys. Lett.* **100**, 162601 (2012).
- ³⁹ L. E. Toth, *Transition metal carbides and nitrides*, Refractory materials, Vol. 7 (Academic Press, New York, 1971) p. 279.
- ⁴⁰ K. Schwarz, *J. Phys. C Solid State Phys.* **8**, 809 (1975).
- ⁴¹ G. M. Eliashberg, *Sov. Phys. - JETP* **34**, 668 (1972).
- ⁴² L. Parlato, R. Latempa, G. Peluso, G. Pepe, R. Cristiano, and R. Sobolewski, *Supercond. Sci. Technol.* **18**, 1244 (2005).
- ⁴³ A. Rothwarf and B. N. Taylor, *Phys. Rev. Lett.* **19**, 27 (1967).
- ⁴⁴ B. Altshuler and A. Aronov, in *Electron-Electron Interact. Disord. Syst.*, Modern Problems in Condensed Matter Sciences, Vol. 10, edited by A. Efros and M. Pollak (North Holland, Amsterdam, New York, 1985) Chap. 1, pp. 1-153.